RESEARCH PAPERS

Acta Cryst. (1995). B51, 650–660

Computational Studies of Crystalline H_3PO_4

BY GRANT R. MOSS,* MOHAMED SOUHASSOU† AND ROBERT H. BLESSING‡

Medical Foundation of Buffalo, 73 High Street, Buffalo, NY 14203, USA

AND ENRIQUE ESPINOSA§ AND CLAUDE LECOMTE

Laboratoire de Minéralogie-Cristallographie et Physique Infrarouge, Faculté des Sciences, Université de Nancy I, URA-CNRS 809, Bôite Postale No. 239, 54506 Vandoeuvre-lès-Nancy CEDEX, France

(*Received* 17 *February* 1994; *accepted* 8 *November* 1994)

Abstract

A polarized split-valence wavefunction was computed for the H_3PO_4 molecule at its neutron crystallographic valence geometry, and the wavefunction was used to map the molecular electron-density distribution and to simulate X-ray crystal structure factors for both static, at-rest and dynamic thermally averaged structures. The thermal vibrational averaging was approximated using anisotropic mean-square atomic displacements from ~300 K neutron diffraction data. The simulated X-ray data were used to test pseudoatom multipole modeling of the valence electron-density distribution, in particular, radial modeling of the *M* valence shell of the P atom, and deconvolution of the nonspherical density features from anisotropic vibrational smearing.

Introduction

We have studied the electron-density distribution and chemical bonding in orthophosphoric acid, H_3PO_4, because it is the prototype for biochemical phosphates, in particular those involved in the ATP cycle of bioenergetics. In this paper we report computational studies based on a polarized split-valence wavefunction for the H_3PO_4 molecule as it occurs in its anhydrous crystals; in an accompanying paper (Souhassou, Espinosa, Lecomte & Blessing, 1995) we report a corresponding experimental analysis.

Occurrences of the H_3PO_4 molecule in the crystalline state include: anhydrous phosphoric acid, H_3PO_4, m.p. 315 K (Furberg, 1955; Smith, Brown & Lehr, 1955; Cole & Peterson, 1964; Cole, 1966; Blessing, 1988, 1989); phosphoric acid hemihydrate, $2H_3PO_4.H_2O$, m.p. 302 K (Smith, Brown & Lehr, 1955; Mighell, Smith & Brown, 1969; Dickens, Prince, Schroeder & Jordan, 1974); a co-crystallized, hydrogen-bonded adduct with acetic acid, $H_3PO_4.CH_3CO_2H$, m.p. 307.5 K (Jönsson, 1972); a strongly hydrogen-bonded, almost ionized adduct with urea, $(H_2N)_2CO.H_3PO_4$ (Sundera-Rao, Turley & Pepinsky, 1957; Wolfram, Arutunian, Antishkina & Porai-Koshits, 1967; Kostansek & Busing, 1972; Mootz & Albrand, 1972; Savage, Blessing & Wunderlich, 1987); and a solvate molecule of crystallization in a dihydrogen phosphate salt of histidine, L-$HisH^+H_2PO_4^-.H_3PO_4$ (Blessing, 1986, 1987).

Previous *ab initio* quantum chemical studies of simple phosphates have investigated: the conformational energetics of H_3PO_4, $H_2PO_4^-$, HPO_4^{2-} and $(CH_3O)_2PO_2^-$ (Newton, 1973; Hayes, Kollman & Rothenberg, 1977); the structure of the 1:1 hydrogen-bonded complex between H_2O and $(CH_3O)_2PO_2^-$ (Alagona, Ghio & Kollman, 1983); the relative stabilities of metal, metal-aquo, metal-diaquo and metal-chloro-aquo complexes of Li^+, Na^+, K^+, Be^{2+}, Mg^{2+} and Ca^{2+} with $H_2PO_4^-$ and $(CH_3O)_2PO_2^-$ (Marynick & Schaefer, 1975); the energetics of hydrolysis of phosphoric and phosphoric–carboxylic anhydride molecules (Hayes, Kenyon & Kollman, 1975, 1978); and the valence and conformational geometry of $OP(OH)_3$ compared with $OP(H)(OH)_2$ and $OP(H)_2OH$ (Ewig & Van Wazer, 1985). These studies employed minimal STO-3G or split-valence 4-31G basis sets, which give reasonable molecular geometries and relative energies, but which are quite inadequate for mapping electron-density distributions. Polarized split-valence 6-31G** basis sets, which are adequate for electron-density mapping, were employed in a study of *ab initio* geometry optimization for

* Present address: Broken Hill Proprietary Ltd., 120 Collins Street, Melbourne, Australia.

† Present address: Laboratoire de Minéralogie-Cristallographie et Physique Infrarouge, Faculté des Sciences, Université de Nancy I, URA-CNRS 809, Bôite Postale No. 239, 54506 Vandoeuvre-lès-Nancy *CEDEX*, France.

‡ To whom correspondence should be addressed.

§ Institut de Ciència de Materials de Barcelona, Consejo Superior de Investigaciones Cientificas, Campus de la Universitat Autonoma de Barcelona, 08193 Bellaterra (Barcelona), Spain.

phosphate species (O'Keefe, Domengès & Gibbs, 1985), but the electron densities were not examined.

In the crystallographic literature on pseudoatom modeling of electron densities, there are numerous results for the first-row biochemical atoms, carbon, nitrogen and oxygen, in their various states of chemical combination, but there are few results for sulfur and even fewer for phosphorus. Phosphorus and sulfur are biologically essential second-row atoms with ten-electron $1s^2 2s^2 2p^6$ [Ne] cores and M valence shells, which are more diffuse than the L valence shells of first-row atoms with two-electron $1s^2$ [He] cores. Often the most difficult aspect of crystallographic pseudoatom modeling has been the stable convergence of the radial parameters of the valence-density fitting functions, and radial modeling of the M valence shell deserves particular attention for studies of phosphate species.

For our study of H_3PO_4, we computed a polarized split-valence molecular wavefunction; used it to simulate X-ray crystal structure factors for both static, at-rest and dynamic thermally averaged structures, and fitted cystallographic pseudoatom models to the simulated data sets in order to compare the electron densities that came from the models with the density that went into the data. Earlier studies of this kind include analysis of simulated dynamic, 123 K data for urea (Swaminathan, Craven, Spackman & Stewart, 1984) and static data for 2-methyl-4-nitroaniline (Howard, Hursthouse, Lehmann, Mallinson & Frampton, 1992). These studies showed that crystallographic pseudoatom models can effectively recover theoretical electron densities, at least for C, H, N, or O structures of first-row atoms with small or zero amplitudes of thermal vibration. In our study of H_3PO_4 we were concerned with modeling the second-row P atom and with deconvolution from thermal smearing at temperatures up to ~300 K.

The H_3PO_4 crystal structure

The non-H structure of anhydrous H_3PO_4 crystals was determined simultaneously and independently by Furberg (1955) and Smith, Brown & Lehr (1955) using two-dimensional photographic X-ray diffraction data. The hydrogen structure of the crystals was determined from three-dimensional neutron diffraction data measured by Cole & Peterson (1964), analyzed by Cole (1966), and re-analyzed by Blessing (1988, 1989). Tables 1 and 2 and Fig. 1 summarize the crystallographic results. The O=P(—OH)$_3$ molecules form strong two-centered P—O—H···O=P hydrogen bonds and weak three-centred P—O—H[···O(H)—P]$_2$ hydrogen bonds. The two-centered bonds and the stronger branches of the three-centered bonds link the molecules into layers parallel to (001); the layers are stacked in van der Waals contacts and cross-linked by the weaker branches of the three-centered bonds. The molecules are crystallographically asymmetric with site symmetry 1 (C_1), and the

Table 1. *Neutron crystallographic data for anhydrous phosphoric acid, as reported by Cole* (1966)

(*a*) Primary crystal data

Chemical formula	H_3PO_4
M_r (dalton)	98
Crystal system	Monoclinic
Space group	$P2_1/c$
a (Å)	5.779 (9)
b (Å)	4.826 (4)
c (Å)	11.61 (4)
β (°)	95.26 (18)
V (Å^3)	322.3 (20)
Z	4
D_x (mg m^{-3})	2.019
Neutron diffraction intensity data	
λ (Å)	1.45
$(\sin\theta_{max})/\lambda$ (Å^{-1})	0.56
No. of unique reflections	482
Least-squares refinement	

The 55 largest $|F_o|^2$ were excluded in order to avoid extinction errors
$R = \sum ||F_o|^2 - |F_c|^2| / \sum |F_o|^2 = 0.058$

(*b*) Fractional atomic coordinates

	x	y	z
H2	0.4762 (4)	0.6202 (4)	0.1771 (2)
H3	−0.1330 (3)	0.4719 (5)	0.1718 (2)
H4	0.2693 (5)	−0.0637 (7)	0.0408 (2)
O1	0.2836 (2)	0.1645 (2)	0.2533 (1)
O2	0.3227 (2)	0.5882 (2)	0.1292 (1)
O3	−0.0567 (2)	0.3411 (2)	0.1196 (4)
O4	0.2749 (2)	0.1319 (3)	0.0342 (1)
P	0.2092 (2)	0.3004 (2)	0.1401 (1)

Table 2. *Neutron crystallographic molecular geometry for* H_3PO_4, *as reported by Cole* (1966)

E.s.d.'s average 0.004 Å for distances and 0.4° for angles.

Bond lengths (Å)		Valence angles (°)		Conformation angles (°)	
P=O1	1.496	O1=P—O2	112.1	O1=P—O2—H	25.2
		O1=P—O3	113.1	O1=P—O3—H	65.8
P—O2	1.546	O1=P—O4	113.3	O1=P—O4—H	34.9
P—O3	1.546				
P—O4	1.550	O2—P—O3	107.2	O3—P—O2—H	149.9
		O2—P—O4	105.7	O4—P—O2—H	−98.6
O2—H	1.015	O3—P—O4	104.9		
O3—H	1.004			O2—P—O3—H	−58.3
O4—H	0.948	P—O2—H	116.6	O4—P—O3—H	−170.3
		P—O3—H	118.2		
		P—O4—H	116.5	O2—P—O4—H	157.9
				O3—P—O4—H	−88.9

The neutron data have been re-analyzed (Blessing, 1988, 1989) with extinction corrections included in a joint refinement with two datasets measured at different wavelengths. This improved the statistics-of-fit and the mean-square displacement parameters, but produced no significant changes in molecular geometry.

H—O—P=O conformation angles and the intermolecular and hydrogen bond geometry depart substantially from idealized $3m$ (C_{3v}) molecular symmetry. Nevertheless, the three P—O(H) bond lengths and the three O=P—O(H), (H)O—P—O(H) and P—O—H valence angles are almost within experimental error of threefold symmetry equivalence. Although the P=O phosphoryl bond is significantly shorter than the P—O(H) phosphohydroxyl bonds, the double bond and single bond notations are merely formal, and both bond types possess partial double-bond character. The O—H and P—O(H)

bond lengths show hydrogen bonding effects: O—H increases substantially and P—O(H) decreases slightly, as the H···O distance decreases (Table 2 and Fig. 1 legend).

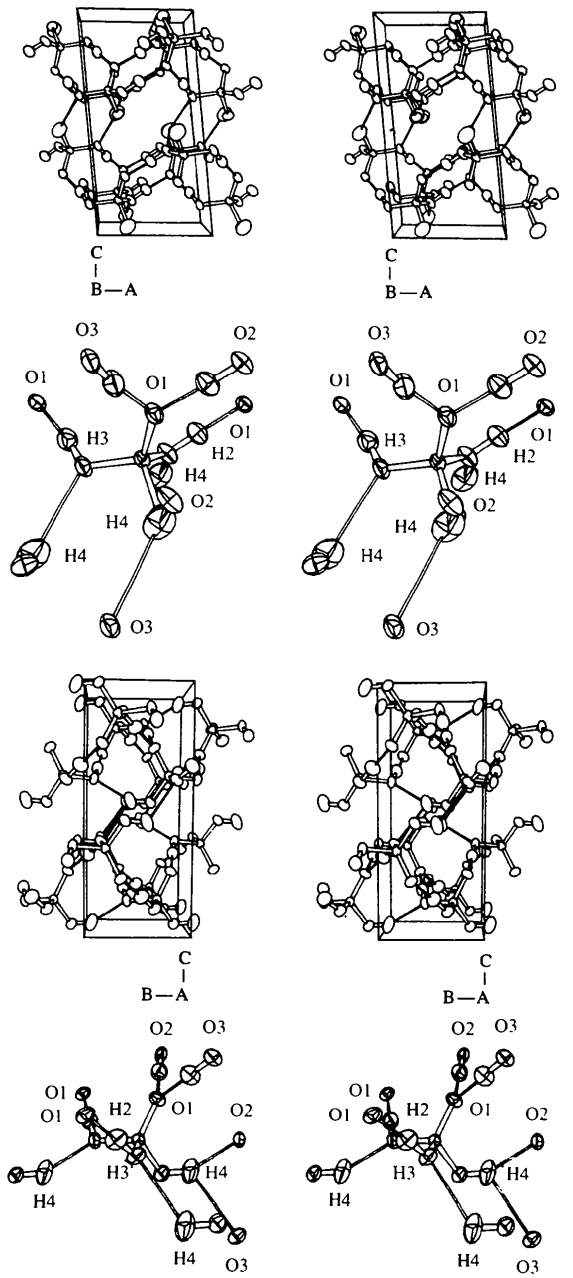

Fig. 1. Stereoscopic drawings (Johnson, 1971) of the crystal and molecular structure of H_3PO_4 (Blessing, 1988, 1989). The orientation of the crystallographic axes in the molecular drawings corresponds to the respective unit-cell drawings, and the thermal vibration ellipsoids are 50% equiprobability surfaces. H2 and H3 are single donors in strong two-centered hydrogen bonds to O1 (1.55 and 1.59 Å H···O and 2.57 and 2.58 Å O···O, respectively); H4 is a double donor in much weaker three-centered hydrogen bonds to O2 and O3 (1.97 and 2.52 Å H···O and 2.85 and 3.10 Å O···O, respectively).

Table 3. *The polarized split-valence basis set for* H_3PO_4

Atom	Primitive set	Contracted set	References	Polarization exponents	References
P	(12*s* 9*p*)	[6*s* 4*p*]	(*a*), (*d*)	*d*, $\zeta = 0.6$	(*a*)
O	(9*s* 5*p*)	[4*s* 3*p*]	(*b*), (*c*)	*d*, $\zeta = 0.75$	(*a*)
H	(4*s*, $\zeta = 1.2$)	[2*s*]	(*c*)	*p*, $\zeta = 0.8$	(*e*), (*f*)

References: (*a*) Rothenberg, Young & Schaefer (1970); (*b*) Dunning (1970); (*c*) Husinaga (1965); (*d*) Veillard (1968); (*e*) Moss (1981); (*f*) Moss & Blessing (1984).

The H_3PO_4 basis set was based on established results for H_2O and for the isoelectronic series SiH_4, PH_3, H_2S and HCl. Polarization functions were d_{xx}, d_{yy}, d_{zz}, d_{xy}, d_{xz}, d_{yz} on the P and O atoms and p_x, p_y, p_z on the H atoms.

Theoretical electron density for H_3PO_4

A wavefunction for an isolated H_3PO_4 molecule, with the neutron crysallographic molecular geometry given in Table 2, was computed using the *ab initio* LCAO–MO–SCF program *HONDO* (Dupuis, Rys & King, 1976) and the polarized split-valence basis set summarized in Table 3. The electron-density distribution calculated (Moss, 1983) from this wavefunction is illustrated in Fig. 2 as sections of the deformation density

$$\Delta\rho(\mathbf{r}) = \rho_m(\mathbf{r}) - \sum_{a=1}^{N} \rho_a^0(\mathbf{r} - \mathbf{r}_a), \qquad (1)$$

where ρ_m is the molecular electron density and ρ_a^0 are spherically averaged, ground-state, free-atom electron densities calculated from the same atomic basis functions. The superposition of the free-atom densities represented by the sum on the right in (1) gives the so-called promolecule density.

Several chemical characteristics of the deformation density shown in Fig. 2 (and in additional maps deposited with the supplementary material*) are worth noting. The chemically distinct P=O and P—OH groups have distinctive electron distributions, and the three O=P—O(—H) and P—O—H bonding regions, and (P—)O(—H) lone-pair regions are essentially chemically equivalent, even though they are not crystallographically equivalent. To close approximations, the densities have local cylindrical symmetry ∞m ($C_{\infty V}$) at the P=O group, in-plane mirror symmetry m (C_s) at each P—O—H group, and threefold rotation and reflection symmetry $3m$ (C_{3V}) at the P atom.

Both bond and lone-pair densities are more diffuse in the P=O group than in the P—O—H groups, and the

*Lists of some computational details, deformation-density maps showing the inadequacy of STO-3G and 4-31G basis sets for realistic density mapping, additional deformation-density maps from the extended basis set wavefunction, residual and deformation-density maps from the pseudoatom fitting, and tables of parameters from the least-squares refinements have been deposited with the IUCr (Reference: CR0475. Copies may be obtained through The Managing Editor, International Union of Crystallography, 5 Abbey Square, Chester CH1 2HU, England.

—O—H densities resemble extended basis-set densities for the water molecule (Hermansson, 1984). The lone-pair densities peak only ~0.2 Å from the O nuclei. The (P—)O(—H) lone pairs appear to occupy a pair of tetrahedral sp^3 hybrid orbitals. The (P=)O lone-pair density is almost circularly symmetric about the P=O axis, and, although there is a slight peaking that suggests trigonal sp^2 hybridization in the O=P—O3(H) plane, it appears that the (P=O)O lone pairs occupy a pair of $p\pi$ orbitals perpendicular to a hybrid $sp\sigma$ orbital.

The P=O and P—O(H) bond densities both peak at 0.5 e Å^{-3}; however, being more diffuse, the P=O density would integrate to a larger electron count than the P—O(H) densities. Moreover, since the P=O bond is ~0.05 Å shorter than the P—O(H) bonds, the difference density along the P=O bond results from

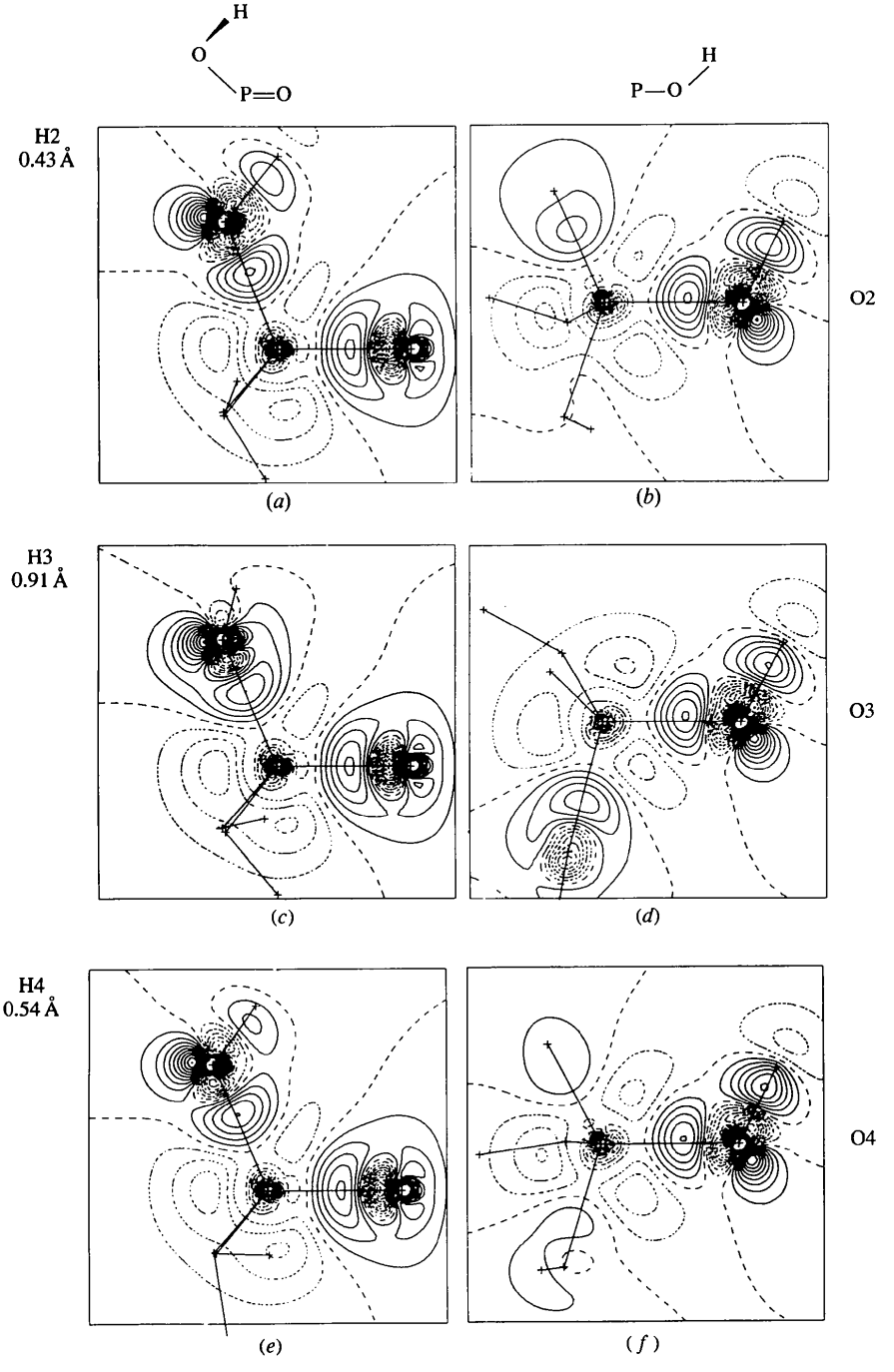

Fig. 2. Static deformation density (1) plotted in the planes: (*a*) (H—)O2—P=O, (*b*) P—O2—H, (*c*) (H—)O3—P=O, (*d*) P—O3—H, (*e*) (H—)O4—P=O and (*f*) P—O4—H. In the (H—)O—P=O sections, the H atom is above the O—P=O plane by the indicated perpendicular distance. Contour interval 0.1 e Å^{-3}; negative contours dotted, zero contour dashed and positive contours solid.

subtraction of higher levels of the overlapping P and O atomic densities. Thus, equal difference-density peak heights in the P=O and P—O(H) bonds imply a higher level of total density in the shorter, stronger P=O bond.

The O2—H, O3—H and O4—H bond densities peak at 0.45, 0.5 and 0.6 e Å^{-3}, respectively [Figs. 2(*d*), (*e*) and (*f*)]. This increase follows the decrease in O—H bond lengths (Table 2), which follows from the increasing strength of H···O hydrogen bonding interactions in the crystals (Fig. 1 legend). Thus, in the O—H bonds not only the total density, but also the difference density increases with decreasing bond length, despite the atomic subtraction effect evident in the P—O bonds.

Apart from their essential role as polarization functions in the LCAO–MO formalism, the role of 3*d* orbitals in phosphorus chemistry has been much discussed for a long time [see, *e.g.* Cruickshank (1961, 1985)]. In the second-row nonmetals P, S and Cl, the 3*d* orbitals are unoccupied in the free-atom ground states, but are energetically accessible for mixing into molecular ground states. This is expressed in qualitative valence bond terms by "expanded octets" for the central atoms in the oxyacids $(HO—)_3P{=}O$, $(HO—)_2S(=O)_2$ and $HO—Cl(=O)_3$, and in this vein, we have discussed bond strengths in H_3PO_4 (Blessing, 1988, 1989) in terms of a simple picture of $p\pi(O) \rightarrow d\pi(P)$ orbital overlap, as originally proposed by Cruickshank (1961). In light of later studies, however, Cruickshank (1985) has concluded that $p\pi \rightarrow d\pi$ bonding plays a relatively minor role in the tetrahedral second-row oxyanions, and that the major role of *d*-basis functions is to move substantial electron density from near the bound atoms into the bond region and thus strengthen the bonding in a very classical way. This *d*-function participation corresponds to *d*-orbital core penetration, which is enhanced for second-row compared with first-row atoms, due to the larger effective nuclear charges in the second-row valence shells. Among the results leading to this interpretation were theoretical deformation densities (Cruickshank & Eisenstein, 1985) for sulfamic acid H_3NSO_3, which is isoelectronic with H_3PO_4, and for which maps of an O=S—N—H section are similar to our O=P—O(H) maps.

Simulated X-ray crystal structure factors from the molecular wavefunction

Following algorithms developed by Stewart (1969), and using a program written by Moss (1983), structure factors were simulated from the molecular wavefunction for a hypothetical static, at-rest H_3PO_4 crystal structure and for dynamic, thermally averaged structures at nominal temperatures of 75, 150 and 300 K. Our simulations were similar to those by Swaminathan, Craven, Spackman & Stewart (1984) for the urea crystal structure at 123 K. The same type of simulation has also been reported for a static 2-methyl-4-nitroaniline crystal structure by Howard, Hursthouse, Lehmann, Mallinson & Frampton (1992).

We emphasize that these simulated structure-factor magnitudes differ, even in principle, from experimentally measurable diffraction data in two important ways: First, static molecular and crystal structures are only imaginary; all real structures are dynamic. Even at extremely low temperatures, real structures undergo at least zero-point vibrational motion, and diffraction experiments yield time and space averages over the vibrational displacements. Second, simulaton from a wavefunction for an isolated molecule yields structure factors for a molecular procrystal rather than a crystal. The simulated data will show artifactual effects of molecular superposition overlap, but not the physical effects of the molecular interactions responsible for crystal binding – except insofar as they affect the 'in-crystal' molecular geometry adopted for computing the *in vacuo* molecular wavefunction.

The thermal averaging of the simulated structure factors

$$F(\mathbf{h}) = \sum_{\text{sym}} \sum_{\mu} \sum_{\nu} P_{\mu\nu} \langle \chi_\mu | \exp(2\pi i\, \mathbf{h} \cdot \mathbf{r}) | \chi_\nu \rangle W_{\mu\nu}(\mathbf{h}) \times \exp(2\pi i \mathbf{h} \cdot \mathbf{R}_{\mu\nu}), \quad (2)$$

was approximated by multiplying each, in general, two-centered (atom *a*, atom *b*) atomic orbital product by an effective two-centered Debye–Waller factor

$$W_{ab}(\mathbf{h}) = \exp\left[-2\pi^2 \sum_{i=1}^{3} \sum_{j=1}^{3} h_i h_j a^{*i} a^{*j} g(U_a^{ij} + U_b^{ij})\right], \quad (3)$$

with $g = 0.5$ corresponding to rigid-rod correlated motions (Stewart, 1969). The thermal vibration tensor components had values $qU^{ij}(\mathbf{T}, \mathbf{L}, \mathbf{S})$, where $U^{ij}(\mathbf{T}, \mathbf{L}, \mathbf{S})$ were as given in Table 4, and on the assumption that $U_{ij} \propto T$, the values $q = 0$, 0.25, 0.5 and 1 were used to simulate a static structure and dynamic structures at $T \approx 75$, 150 and 300 K, respectively.

Equations (2) and (3) approximate the thermodynamic ensemble average over all nuclear configurations (Stewart & Feil, 1980) from the wavefunction for the thermal mean equilibrium configuration in a very straightforward manner (Stewart, 1969). Other approximations have also been described (Ruysink & Vos, 1974; Stevens, Rys & Coppens, 1977).

The atomic-mass-weighted average of the U^{ii} values from Table 4 gives an overall isotropic mean-square vibrational displacement $\langle u^2 \rangle \approx 0.025$ Å^2 at $T \approx 300$ K. Using the Debye relation

$$\langle u^2 \rangle = 3h^2T/(4\pi^2 k_B m \Theta_D{}^2), \quad T > \Theta_D, \quad (4)$$

which is in principle applicable only to cubic monoatomic crystals (*e.g.* Willis & Pryor, 1975, pp. 122 ff.), and taking *m* to be the molecular mass, we estimate a

Table 4. U^{ij} (T,L,S) *values* (Å^2) *calculated from a rigid-body fit* (*Schomaker & Trueblood*, 1968) *to the independent-atom* U^{ij} *values* (*Blessing*, 1988, 1989) *for the non-*H *atoms of* H_3PO_4 *from room-temperature* (~ 300 K) *neutron diffraction data*

	U^{11}	U^{22}	U^{33}	U^{12}	U^{13}	U^{23}
H2	0.0317	0.0261	0.0471	−0.0104	−0.0158	0.0076
H3	0.0220	0.0509	0.0458	0.0137	−0.0033	−0.0154
H4	0.0502	0.0231	0.0440	0.0072	0.0089	−0.0108
O1	0.0225	0.0292	0.0250	−0.0017	−0.0037	0.0070
O2	0.0290	0.0175	0.0337	−0.0027	−0.0111	0.0032
O3	0.0177	0.0322	0.0310	0.0037	−0.0068	−0.0079
O4	0.0365	0.0244	0.0281	0.0043	0.0077	−0.0052
P	0.0170	0.0165	0.0202	0.0015	−0.0025	−0.0014

Table 5. *Contributions to the static, at-rest and dynamic* ~ 300 K *thermally averaged theoretical values of* $F(313)$

One-center terms	Static Re	Static Im*	Dynamic Re	Dynamic Im*	Atomic Debye–Waller factor $\exp(-\mathbf{h}^T\beta\mathbf{h})$ at ~300 K
H2	0.040	0.113	0.035	0.098	0.867
H3	0.008	0.121	0.006	0.096	0.794
H4	−0.124	−0.023	−0.083	−0.015	0.667
O1	−3.428	1.585	−2.899	1.341	0.846
O2	−3.445	−2.106	−2.959	−1.809	0.859
O3	1.713	3.394	1.509	2.990	0.881
O4	−0.825	−3.579	−0.609	−2.640	0.738
P	8.524	0.022	7.539	0.020	0.884
One-centre totals	2.463	−0.473	2.539	0.081	
Two-centre totals	−0.359	0.296	−0.282	0.294	
Molecular totals	2.104	−0.177	2.257	0.375	

* The tabulated contributions are those from the crystallographically independent molecule. Since the crystal structure has a centre of symmetry at the origin, the imaginary components sum to zero when the contributions from the centrosymmetrically equivalent molecule are added.

Debye temperature $\Theta_D \approx 130$ K for H_3PO_4 crystals. This would mean that $U^{ij} \propto T$ is a reasonable assumption for our $q = 1$ (300 K) and $q = 0.5$ (150 K) simulated data, but doubtful for the $q = 0.25$ (75 K) data.

We were surprised to find that a few structure-factor magnitudes actually *increased* slightly with increasing thermal motion. An example of this apparently counter-intuitive result is shown in Table 5, which summarizes a test calculation of the static ($q = 0$) and dynamic ($q = 1$) structure factors for the (313) reflection. For each atom, the magnitude of the dynamic one-center term is smaller than that of the corresponding static term, because the dynamic term has been multiplied by an atomic Debye–Waller factor, $0 < W < 1$. Nevertheless, the (real) one-center total is slightly larger for the dynamic than for the static terms, because the totals are sums of signed terms, each of which is multiplied by a different Debye–Waller factor.

On reflection, we realized that the same type of effect can occur in conventional crystallographic calculations of the structure factors, $F(\mathbf{h}) = \sum_{a=1}^{N} f_a(\mathbf{h}) \exp(2\pi i\, \mathbf{h}^T\mathbf{r}_a - \mathbf{h}^T\beta_a\mathbf{h})$, where $\beta^{ij} = 2\pi^2 a^{*i} a^{*j} Uij$. With increasing thermal motion, all the atomic Debye–Waller factors necessarily decrease because the β matrices are positive definite; however, a decrease in $|F(\mathbf{h})|$ is an analytical requirement only if the Debye–Waller factors are the same for all atoms and factor out of the vectorial atomic summation. In general, and on average, $|F(\mathbf{h})|$ decrease, but exceptionally individual values may increase slightly.

Pseudoatom modeling of the electron density

The simulated structure factor data were fitted using the program *MOLLY* (Hansen & Coppens, 1978), which employs generalized atomic scattering factors that are the Fourier transforms of pseudoatom electron densities parameterized to model nonspherical electron redistributions due to chemical bonding (Coppens, 1993; Coppens & Becker, 1992; Maslem, Fox & O'Keefe, 1992). Each bound pseudoatom is modeled by a multipolar expansion about the free atom

$$\rho(\mathbf{r}) = \rho_c(r) + P_v\kappa_0^3\rho_v(\kappa_0 r) + \kappa_1^3 \sum_{l=0}^{l_{max}} R_l(\kappa_l r) \sum_{m=-1}^{+l} P_{lm} y_{lm}(\theta, \varphi), \qquad (5)$$

where ρ_c is the spherically symmetric Hartree–Fock core electron density, ρ_v is the spherically averaged free- atom Hartree–Fock valence electron density normalized to one electron, y_{lm} are real spherical harmonic angular functions normalized such that $|y_{lm}|$ integrates to $2 - \delta_{01}$, and R_l are Slater-type radial functions normalized to unity

$$R_l(r) = \alpha^{n+3}/(n+2)!\, r^n e^{-\alpha r}, \quad n = n_l \geq l. \qquad (6)$$

The κ_0 and κ_1 are dimensionless radial scaling coefficients (Coppens, Guru Row, Leung, Stevens, Becker & Yang, 1979) that allow for contraction ($\kappa > 1$) or expansion ($\kappa < 1$) of the spherical valence shell and the directed valence multipoles, respectively. The r, θ and φ coordinates refer to local atom-centered Cartesian axes; this facilitates imposition of local noncrystallographic chemical symmetry constraints to reduce the number of variable parameters. The variable electron-distribution parameters are the populations P_v and P_{lm}, and the contraction–expansion coefficients κ_0 and κ_1. Since the y_{lm} with $l > 0$ integrate to zero, net atomic charges are given by $q = N_v - (P_v + P_{00})$, where N_v is the neutral-atom number of valence electrons; unit-cell electrical neutrality is maintained by requiring that $\sum_a \Delta q_a = 0$ in each least-squares cycle (Coppens, 1977).

Pseudoatom models were fitted by least-squares minimization of $\chi^2 = \sum w\Delta^2$, where $\Delta = |F_o| - k^{-1}|F_c|$ and $w = 1$, since the simulated F_o data were 'error free'. The scale factor k was included to allow for numerical correlation with the vibrational parameters, but in all cases k converged to values that

differed from unity by less than 0.003. Agreement statistics were the conventional crystallographic residual $R = \sum|\Delta|/\sum|F_o|$, the normalized r.m.s. error-of-fit $R_w = [\chi^2/\sum w|F_o|^2]^{1/2}$, and the standardized r.m.s. error-of-fit $Z = [\chi^2/(n-m)]^{1/2}$, where $n = 2698$ unique reflection data to $d_{min} = \lambda/(2\sin\theta_{max}) = 0.5$ Å, and $m = 170$ parameters, of which 124 were pseudoatom parameters. Since $w = 1$ for the simulated data, we expect $Z \to 0$ at convergence, rather than $Z \to 1$ as we should expect with $w = 1/\sigma^2(|F_o|)$ for experimental data.

The only noncrystallographic constraint imposed on the pseudoatoms was that only four values of κ_0 and κ_1 were fitted, *viz.* for the four chemically distinct atom types P, O1, O2 (=O3 = O4) and H2 (= H3 = H4). The P_v population parameters were deemed sufficient for describing interatomic charge transfers, and the $l = 0$ valence monopole populations were fixed at $P_{00} = 0$. Atomic scattering factors for the core and valence shells of the spherically averaged free atoms were from the HF–SCF calculations of Clementi (1965).

The valence multipole expansions extended to $l_{max} = 4$, 3 and 2, *i.e.* hexadecapoles, octupoles and quadrupoles, for the P, O and H atoms, respectively. Pre-exponential radial orders $n_l \geq l$ for the $l = 1, 2, \ldots, l_{max}$ multipoles were $N_l = 6, 6, 7, 7$ for P; 2, 2, 3 for O; and 1, 2 for H. The rationale for these choices is discussed below. Radial exponential coefficients for P, O and H were $\alpha = 3.5$, 4.5 and 2.3 bohr^{-1}, respectively, which are approximately twice the valence-shell-averaged orbital exponents from the HF–SCF atomic ground state wavefunctions of Clementi & Raimondi (1963).

The least-squares refinements were carried out in a sequence of 13 three-cycle stages. Throughout, the x_i and U^{ij} parameters of the H atoms were held fixed at their values (Tables 1 and 4) from the experimental neutron analysis. At each stage the varied parameters were *k* and: (1) P_v, (2) κ_0, (3) P_v, (4) κ_0, (5) P_{lm}, (6) κ_1, (7) P_{lm}, (8) $P_v + P_{lm}$, (9) $P_v + P_{lm}$ + non-H x_i and U^{ij}, (11) $\kappa_0 + \kappa_1$, (12) $P_v + P_{lm}$ + non-H x_i and U^{ij}, and, finally (13) all parameters except the H atom x_i and U^{ij}.

Radial modeling for the phosphorus pseudoatom

Since few pseudoatom analyses of phosphate molecules have been performed (Swaminathan & Craven, 1984; Hansen, Protas & Marnier, 1991; Klooster & Craven, 1992; Klooster, 1992; Streltsov, Belokoneva, Tsirelson & Hansen, 1993), we used the simulated static structure factors to investigate radial modeling of the phosphorus pseudoatom.

The Slater-type radial density functions (6), with *r* replaced by $\kappa_1 r$, give multipole maxima ($dR_l/dr = 0$) at radii $r_{max\,l} = n_l/(\alpha\kappa_1)$, which depend on the chosen orders n_l of the pre-exponential factor r^n as well as on the chosen exponential coefficients α and fitted κ_1 values. Table 6 lists suitable choices for α values and Table 7

Table 6. *Exponential coefficients* α (bohr^{-1}) *for Slater-type radial-density functions* (6) *from averaged orbital exponents* ζ *from wavefunctions for HF–SCF free atoms (Clementi & Raimondi, 1963) and STO–NG small molecules (Hehre, Ditchfield, Stewart & Pople, 1969)*

$\alpha = 2\zeta$ since $\rho \propto |\psi|^2$.

Valence shell	Atom	Free-atom α	Molecule-optimized α
K-shell	H	2	2.48
	He	3.38	3.38
L-shell	Li	1.28	1.60
	Be	1.91	2.30
	B	2.52	3.00
	C	3.18	3.42
	N	3.84	3.90
	O	4.47	4.50
	F	5.11	5.10
	Ne	5.76	5.76
M-shell	Na	1.67	3.50
	Mg	2.20	3.40
	Al	2.73	3.40
	Si	3.06	3.46
	P	3.46	3.80
	S	3.85	4.10
	Cl	4.26	4.20
	Ar	4.67	4.66

The differences between the free-atom and molecule-optimized values are large for H and the metallic elements, the valence shells of which are strongly contracted in the bound atoms. The differences are much smaller for the nonmetals, and they vanish for the noble gases.

Table 7. *Values of* $n = n_l$, *as suggested by Hansen & Coppens* (1978) *for Slater-type density-radial functions* [(6) *and* (7)]

Orbital product $n'l'$ $n''l''$	Density multipole $R_l\, y_{lm}$	Multipole order l	Density radial pre-exponential $r^n = r^{n'+n''-2}$
2*s* 2*s*	Monopole	0	r^2
2*s* 2*p*	Dipole	1	r^2
2*p* 2*p*	Quadrupole	2	r^2
2*p* 3*d*	Octupole	3	r^3
3*d* 3*d*	Hexadecapole	4	r^4

gives n_l values, as suggested by Hansen & Coppens (1978). The suggested *n* values are based on

$$r^n = r^{n'-1} r^{n''-1} = r^{n'+n''-2} \qquad (7)$$

for density functions corresponding to products $(\psi^*_{n'l'}\,\psi_{n''l''})$ of Slater orbital wavefunctions $\psi_{n'l'}(r,\theta,\varphi) = N_{n'l'}\, r^{n'-1}\, e^{-\zeta r} Y_{l'm'}(\theta,\varphi)$, which have pre-exponential radial dependence $r^{n'-1}$ by analogy with hydrogenic orbitals. The suggested values $n_l = 2, 2, 2, 3, 4$ for $l = 0, 1, 2, 3, 4$ satisfy the condition $n_l \geq 1$, which is required for proper Coulombic behavior satisfying Poisson's equation as $r \to 0$ (Stewart, 1977). These n_l values have been found suitable for first-row atoms in numerous studies, and we adopted them for the O and H atoms.

For second-row atoms such as phosphorus, $n' = n'' = 3$ for all valence orbitals, and the orbital product scheme (7) suggests $n_l = 4$ for $l = 0$–4. These n_l

are, however, too small for the P atom in H_3PO_4, as shown in Fig 3(*a*) by a map of the residual density

$$\Delta\rho(\mathbf{r}) = V^{-1}\sum_{\mathbf{h}}(k|F_o| - |F_c|)\exp(i\varphi_c - 2\pi i\,\mathbf{h}\cdot\mathbf{r}), \quad (8)$$

after a fit to the simulated static data. An extensive series of fitting trials, using different sets of n_l for the P atom and seeking to minimize the residual density, led finally to the set $n_l = 6, 6, 7, 7$ for $l = 1, 2, 3, 4$. Residual density features from this set, shown in Fig. 3(*b*), were reduced to levels comparable to usual levels of random experimental error. Of course, changing the n_l values changed the fitted value of $\kappa_1\alpha$: Expansion of the valence multipoles due to the larger n_l was balanced by contraction due to a larger $\kappa_1\alpha$.

Recovery of the theoretical electron density

With the empirically optimized n_l values for phosphorus, the fit to the static simulated data gave the static deformation-density maps shown in Fig. 4. These maps show representative sections of the function

$$\Delta\rho(\mathbf{r}) = \sum_{a=1}^{N}\rho_a(\mathbf{r} - \mathbf{r}_a) - \rho_a^0(\mathbf{r} - \mathbf{r}_a), \quad (9)$$

where the ρ_a are pseudoatom-modeled densities (4), and the ρ_a^0 are spherically averged HF–SCF free-atom densities. The function (9) from the pseudoatom model is to be compared with (1) from the molecular wavefunction.

The close similarity of Figs. 4(*a*) and (*b*) to Figs. 2(*a*) and (*b*) shows how well the pseudoatom modeling recovers the wavefunction density that was incorporated into the simulated structure factors. The most noteworthy of the small differences between the two sets of maps are: (1) Sharp features very close to (~ 0.1 Å from) the P and O nuclear positions in the infinite-resolution wavefunction maps are not reproduced in the finite-resolution [$d_{\min} = \lambda/(2\sin\theta_{\max}) = 0.5$ Å] pseudoatom maps. (2) The density along the O—H bonds peaks ~ 0.2 e Å^{-3} higher and ~ 0.15 Å closer to the H atom in the pseudoatom maps than in the wavefunction maps. This is because a spherically contracted ($\zeta = 1.15$ bohr^{-1}) H atom (Stewart, Davidson & Simpson, 1965) was subtracted from the pseudoatom density, while an uncontracted ($\zeta = 1$ bohr^{-1}) H atom was subtracted from the wavefunction density. (3) Peak densities along the P=O and P—O(H) bonds and in the (P—)O(—H) atom lone-pair regions are ~ 0.1 e Å^{-3} lower from the pseudoatom fit than from the wavefunction. This may be at least partly because Gaussian approximations to free-atom densities were subtracted from the Gaussian wavefunction density, while HF–SCF atomic densities were subtracted from the pseudoatom-modeled density.

Deconvolution of nonspherical electron distribution from anisotropic vibrational smearing

The maps shown in Fig. 4 resulted from the 13-stage pseudoatom fit to the simulated static data, with the atomic positional parameters fixed at the experimental neutron diffraction values (Table 2) and the vibrational displacement parameters fixed at zero. To test the deconvolution from anisotropic thermal smearing, the pseudoatom model from the fit to the simulated static data was used as a starting point for refinements with the

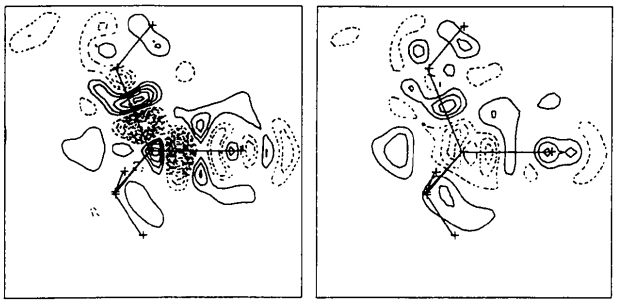

(*a*) (*b*)

Fig. 3. Residual density (8) in the (H—)O2—P=O plane after pseudoatom fitting to the simulated static structure factor data with two different sets of n_l values for the phosphorus pseudoatom.

n_l (P) $l = 1, 2, 3, 4$	R	R_w	Z	k^{-1}	$\kappa_1\alpha$ (P)
(*a*) 4, 4, 4, 4	0.0040	0.0041	0.06	0.9995	2.96 bohr^{-1}
(*b*) 6, 6, 7, 7	0.0032	0.0035	0.05	0.9988	4.18

The two fitted values of $\kappa_1\alpha$ bracket both the valence-shell averaged value $2\zeta = 3.46$ bohr^{-1} for a free, ground state, HF–SCF P atom (Clementi & Raimondi, 1963) and the standard molecule-optimized value $2\zeta = 3.80$ bohr^{-1} for STO–NG P atoms (Hehre *et al.*, 1969). Our pseudoatom-optimized value $\kappa_1\alpha = 4.18$ bohr^{-1} with $n_l = 6, 6, 7, 7$ for $l = 1, 2, 3, 4$ in fact agrees closely with the molecule-optimized value $2\zeta = 4.06$ bohr^{-1} obtained by Hehre *et al.* (1969) from STO-3G and STO-4G calculations for H_3PO_4. Contour interval 0.025 e Å^{-3}; zero contour omitted, negative contours dotted and positive contours solid. (*a*) $-0.28 \le \Delta\rho \le +0.14$ and $\sigma(\Delta\rho) = 0.021$; (*b*) $-0.09 \le \Delta\rho \le +0.09$ and $\sigma(\Delta\rho) = 0.014$ e Å^{-3}.

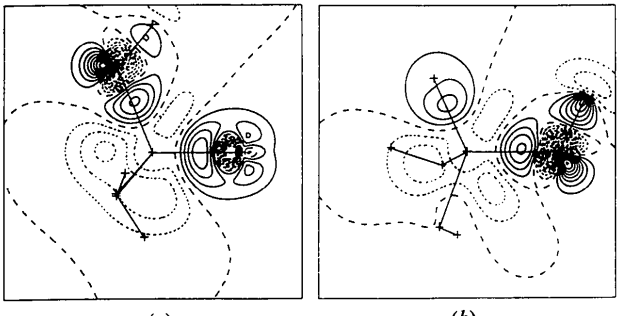

(*a*) (*b*)

Fig. 4. Static deformation density (9) in the planes (*a*) (H—)O2—P=O and (*b*) P—O2—H from our best pseudoatom fit [Fig. 3(*b*)] to the simulated static structure factors. Contours as in Fig. 2. Compare with Figs. 2(*a*) and (*b*).

simulated 75, 150 and 300 K dynamic data. These refinements were begun with a refinement of the U^{ij} of all atoms – including H atoms – with the positional and pseudoatom density parameters fixed. This was then followed by the 13-stage pseudoatom refinement. The pseudoatom parameters, which are tabulated in the deposited supplementary material, remained very stable in these refinements, as can be seen by comparing Figs. 5(*a*), (*c*) and (*e*) with Fig. 4(*a*). U^{ij} also refined to proper values, as indicated in Table 8. The fitted U^{ij} differed from the values given in Table 4 by at most $\sim 1\%$ for the non-H atoms and $\sim 10\%$ for the H atoms.

As a further test of the deconvolution, each of the simulated dynamic data sets was independently treated

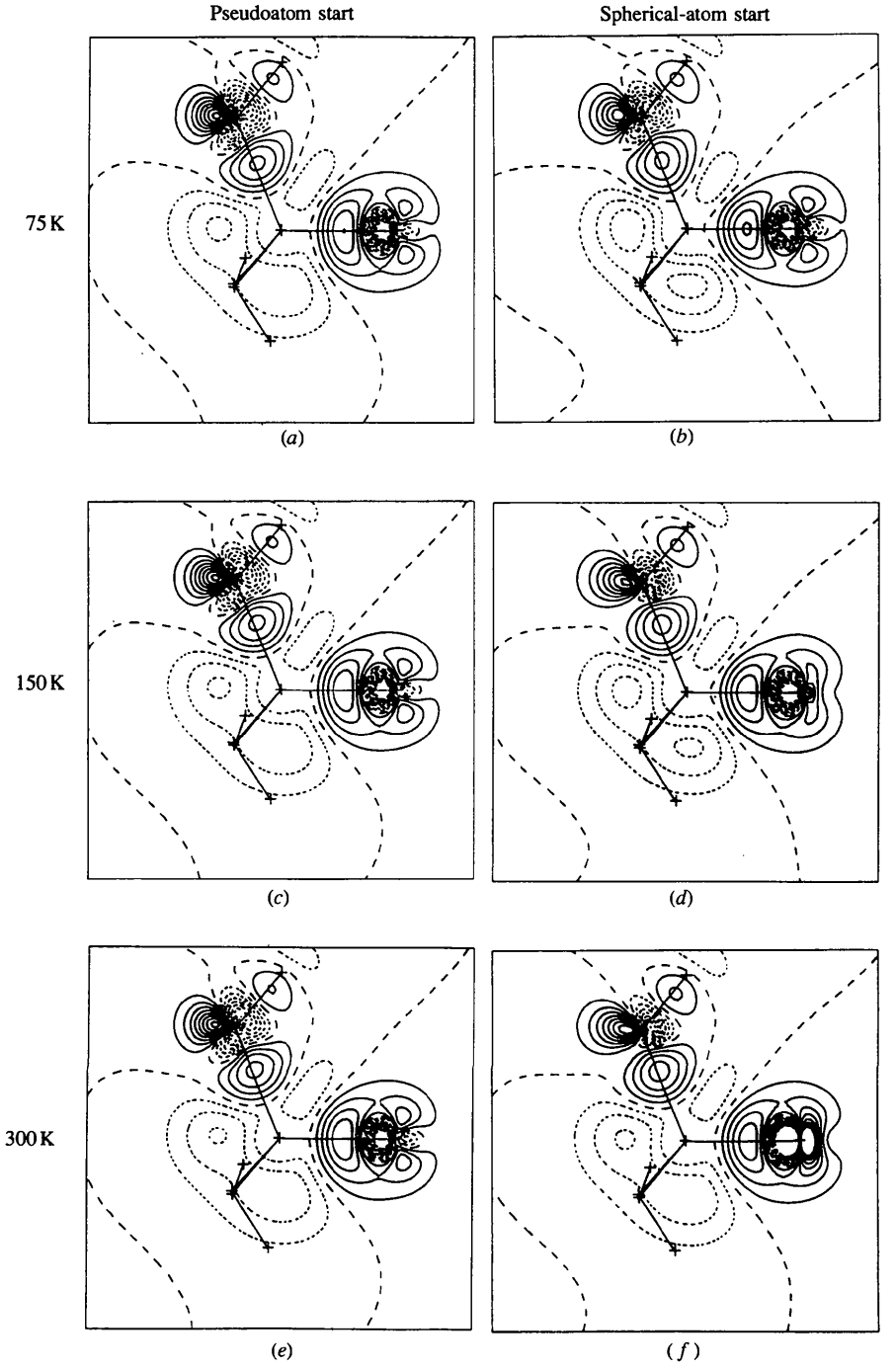

Fig. 5. Static deformation density (9) in the (H—)O2—P=O plane after pseudoatom fitting to the simulated dynamic structure factor data: (*a*) and (*b*) 75 K, (*c*) and (*d*) 150 K, and (*e*) and (*f*) 300 K. Contours as in Fig. 2. For refinements (*a*), (*c*) and (*e*) the starting model was the pseudoatom model fitted to the simulated static data. For refinements (*b*), (*d*) and (*f*) the starting model was a spherical-atom model fitted to the respective simulated dynamic data set.

Static pseudoatom start

T (K)		R	R_w	Z	k^{-1}
75	(*a*)	0.0029	0.0034	0.04	0.9981
150	(*c*)	0.0030	0.0031	0.03	0.9979
300	(*e*)	0.0030	0.0029	0.02	0.9976

Dynamic spherical-atom start

T (K)		R	R_w	Z	k^{-1}
75	(*b*)	0.0037	0.0040	0.05	0.9980
150	(*d*)	0.0030	0.0032	0.03	0.9979
300	(*f*)	0.0028	0.0027	0.02	0.9972

Table 8. *Changes from the rigid-body mean-square displacement parameters (Table 4) after refinement with the simulated (~ 300 K) dynamic structure factors*

$\Delta^{ij} = U^{ij}$ (refined) $- U^{ij}$(T, L, S) (Å^2).

(*a*) Static pseudoatom start

	Δ^{11}	Δ^{22}	Δ^{33}	Δ^{12}	Δ^{13}	Δ^{23}
H2	0.0013	−0.0031	−0.0035	0.0015	0.0016	0.0002
H3	−0.0003	−0.0049	−0.0036	−0.0030	−0.0016	0.0014
H4	−0.0042	0.0006	−0.0058	−0.0012	0.0009	0.0014
O1	−0.0001	0.0000	−0.0001	0.0000	0.0000	0.0000
O2	0.0000	0.0000	0.0000	0.0000	−0.0001	0.0000
O3	0.0000	0.0000	−0.0001	0.0000	0.0000	−0.0001
O4	0.0000	−0.0001	−0.0001	0.0000	0.0000	0.0000
P	−0.0001	−0.0001	−0.0001	0.0000	0.0000	0.0000

(*b*) Dynamic spherical-atom start (H atoms fixed)

	Δ^{11}	Δ^{22}	Δ^{33}	Δ^{12}	Δ^{13}	Δ^{23}
O1	−0.0001	−0.0003	−0.0001	0.0001	0.0001	−0.0002
O2	−0.0002	0.0000	0.0002	−0.0002	−0.0003	−0.0001
O3	−0.0003	0.0001	0.0002	0.0002	0.0001	−0.0002
O4	0.0002	−0.0003	0.0001	0.0000	0.0001	−0.0002
P	−0.0001	−0.0001	−0.0001	0.0000	0.0000	0.0000

just as the experimental H_3PO_4 data set described in the accompanying paper (Souhassou, Espinosa, Lecomte & Blessing, 1995): With the H atom x_i and U^{ij} fixed at their neutron diffraction values, the non-H atom x_i and U^{ij} were refined, starting from the neutron values and fitting the spherical-atom model to the high-angle data with $(\sin\theta)/\lambda \geq 0.8$ Å^{-1}. The 13-stage pseudoatom refinements were then carried out from the spherical-atom starting points. U^{ij} again refined properly, as indicated in Table 8, and the pseudoatom model gave very much the same results as the earlier refinements, as can be seen in Figs. 5(*b*), (*d*) and (*f*). The most noticeable difference was the strong, tight density dipole that developed at the O1 atom of the P=O phosphoryl group in the fit to the simulated 300 K data [Fig. 5(*f*)]. This corresponded to the O atom refining to a false position 0.00037 Å too close to the P atom, as shown in Table 9. This tendency was also just barely perceptible in the fit to the simulated 150 K data, which gave a much smaller tight dipole at O1 [Fig. 5(*d*)] and shortened P=O by 0.0008 Å (Table 9).

Apart from these small correlated errors in the position and the dipolar deformation density of the phosphoryl O atom, the pseudoatom model very effectively recovered the theoretical electron density that went into the calculation of the simulated structure factors. The multipolar valence-density features were effectively deconvoluted from anisotropic vibrational smearing, even up to $T \approx 300$ K at which temperature the r.m.s. atomic displacement in crystalline H_3PO_4 is $\langle u^2 \rangle^{1/2} \approx 0.16$ Å.

We thank Professors Robert Stewart and Harry King for helpful discussions. We are also grateful for the support of this research by USDHHS PHS NIH grants GM34073 (RHB, MS and CL) and DK19856 (GRM and RHB) and by a project grant DGICYT PB90-0134 and a fellowship from the Commissionat per a Universitats Recerca de la Generalitat de Catalunya (EE).

Table 9. *Bond lengths* (Å) *in the hypothetical static* H_3PO_4 *molecule and changes from them* (Å) *after first spherical-atom then pseudoatom refinements with the simulated structure factors*

	Fixed bond lengths	Refined changes		
	Static	75 K	150 K	300 K
P=O1	1.4958	0.0003	−0.0008	−0.0037
P—O2	1.5461	0.0007	0.0005	0.0005
P—O3	1.5458	0.0007	0.0005	0.0003
P—O4	1.5497	0.0009	0.0007	0.0007
O2—H	1.0146	−0.0001	−0.0006	−0.0005
O3—H	1.0044	−0.0001	−0.0006	−0.0003
O4—H	0.9479	−0.0002	−0.0006	−0.0005

References

ALAGONA, G., GHIO, C. & KOLLMAN, P. (1983). *J. Am. Chem. Soc.* **105**, 5226–5230.

BLESSING, R. H. (1986). *Acta Cryst.* B**42**, 613–621.

BLESSING, R. H. (1987). *Acta Cryst.* B**43**, 407.

BLESSING, R. H. (1988). *Acta Cryst.* B**44**, 334–340.

BLESSING, R. H. (1989). *Acta Cryst.* B**45**, 200.

CLEMENTI, E. (1965). *IBM J. Res. Dev.* **9**, Suppl. As tabulated by R. F. STEWART & M. A. SPACKMAN (1983). *VALRAY Users' Manual.* Carnegie-Mellon Univ., Pittsburgh, Pennsylvania.

CLEMENTI, E. & RAIMONDI, D. L. (1963). *J. Chem. Phys.* **38**, 2686–2689. As cited by M. KARPLUS & R. N. PORTER (1970). *Atoms and Molecules*, p. 230. New York: W. A. Benjamin, Inc.

COLE, F. E. (1966). PhD Thesis, Univ. of Washington, Pullman. Ann Arbor, Michigan: University Microfilms International.

COLE, F. E. & PETERSON, S. W. (1964). *Am. Cryst. Assoc. Meeting*, Montana State Univsity, Bozeman, July 1964, Abstract No. H-5.

COPPENS, P. (1977). *Israel J. Chem.* **16**(2–3), 159–162.

COPPENS, P. (1993). In *International Tables for Crystallography*, Vol. B, Ch. 1.2. Dordrecht: Kluwer Academic Publishers.

COPPENS, P. & BECKER, P. (1992). In *International Tables for Crystallography*, edited by A. J. C. WILSON, Vol. C, pp. 627 ff. Dordrecht: Kluwer Academic Publishers.

COPPENS, P., GURU ROW, T. N., LEUNG, P., STEVENS, E. D., BECKER, P. J. & YANG, Y. W. (1979). *Acta Cryst.* A**35**, 63–72.

CRUICKSHANK, D. W. J. (1961). *J. Chem. Soc.* **1961**, 5485–5504.

CRUICKSHANK, D. W. J. (1985). *J. Mol. Struct.* **130**, 177–191.

CRUCKSHANK, D. W. J. & EISENSTEIN, M. (1985). *J. Mol. Struct.* **130**, 143–156.

DICKENS, B., PRINCE, E., SCHROEDER, L. W. & JORDAN, T. H. (1974). *Acta Cryst.* B**30**, 1470–1473.

DUNNING, T. H. (1970). *J. Chem. Phys.* **53**, 2823.

DUPUIS, M., RYS, J. & KING, H. F. (1976). *HONDO*76, *QCPE*336 and -338. Indiana Univ., Bloomington.

EWIG, C. S. & VAN WAZER, J. R. (1985). *J. Am. Chem. Soc.* **107**, 1965–1971.

FURBERG, S. (1955). *Acta Chem. Scand.* **9**, 1557–1566.

HANSEN, N. K. & COPPENS, P. (1978). *Acta Cryst.* A**34**, 909–921.

HANSEN, N. K., PROTAS, J. & MARNIER, G. (1991). *Acta Cryst.* B**47**, 660–672.

HAYES, D. M., KENYON, G. L. & KOLLMAN, P. A. (1975). *J. Am. Chem. Soc.* **97**, 4762–4763.

HAYES, D. M., KENYON, G. L. & KOLLMAN, P. A. (1978). *J. Am. Chem. Soc.* **100**, 4331–4340.

HAYES, D. M., KOLLMAN, P. A. & ROTHENBERG, S. (1977). *J. Am. Chem. Soc.* **99**, 2150–2154.

HEHRE, W. J., DITCHFIELD, R., STEWART, R. F. & POPLE, J. A. (1969). *J. Chem. Phys.* **52**, 2769–2773.

HERMANSSON, K. (1984). *Acta Universitatis Upsaliensis*, p. 744. Doctoral Dissertation, Univ. of Uppsala.

HOWARD, S. T., HURSTHOUSE, M. B., LEHMANN, C. W., MALLINSON, P. R. & Frampton, C. S. (1992). *J. Chem. Phys.* **97**, 5616–5630.

HUZINAGA, S. (1965). *J. Chem. Phys.* **42**, 1293.
JOHNSON, C. K. (1971). *ORTEP*II. Report ORNL-3794, revised. Oak Ridge National Laboratory, Tennessee, USA.
JÖNSSON, P.-G. (1972). *Acta Chem. Scand.* **26**, 1599–1619.
KLOOSTER, W. T. (1992). PhD Thesis, Universitiet Twente, Enschede, The Netherlands.
KLOOSTER, W. T. & CRAVEN, B. M. (1992). *Biopolymers*, **32**, 1141–1154.
KOSTANSEK, E. C. & BUSING, W. R. (1972). *Acta Cryst.* B**28**, 2454–2459.
MARYNICK, D. S. & SCHAEFER, H. F. (1975). *Proc. Natl Acad. Sci. USA*, **72**, 3794–3798.
MASLEN, E. N., FOX, A. G. & O'KEEFE, M. A. (1992). In *International Tables for Crystallography*, edited by A. J. C. WILSON, Vol. C, pp. 476 ff. Dordrecht: Kluwer Academic Publishers.
MIGHELL, A. D., SMITH, J. P. & BROWN, W. E. (1969). *Acta Cryst.* B**25**, 776–781.
MOOTZ, D. & ALBRAND, K.-R. (1972). *Acta Cryst.* B**28**, 2459–2463.
MOSS, G. R. (1981). *Acta Cryst.* A**37**, C-137. XIIth IUCr Congress, Ottawa, August 1981, Abstract No 06.7-03.
MOSS, G. R. (1983). *MOLDEN* and *MOLSF. Programs for Calculating Electron Densities and X-ray Structure Factors from a HONDO. Wavefunction.* Medical Foundation of Buffalo, Buffalo, New York.
MOSS, G. R. & BLESSING, R. H. (1984). *Acta Cryst.* A**40**, C-157. XIIIth IUCr Congress, Hamburg, August 1984, Abstract No. 06.2-1.
NEWTON, M. D. (1973). *J. Am. Chem. Soc.* **95**, 256–258.
O'KEEFE, M., DOMENGÈS, B. & GIBBS, G. V. (1985). *J. Phys. Chem.* **89**, 2304–2309.
ROTHENBERG, S., YOUNG, R. H. & SCHAEFER, H. F. (1970). *J. Am. Chem. Soc.* **92**, 3243.
RUYSINK, A. F. J. & VOS, A. (1974). *Acta Cryst.* A**30**, 497–502.
SAVAGE, H. F. J., BLESSING, R. H. & WUNDERLICH, H. (1987). *Trans. Am. Cryst. Assoc.* **23**, 97–100.
SCHOMAKER, V. & TRUEBLOOD, K. N. (1968). *Acta Cryst.* B**24**, 63–76.
SMITH, J. P., BROWN, W. E. & LEHR, J. R. (1955). *J. Am. Chem. Soc.* **77**, 2728–2730.
SOUHASSOU, M., ESPINOSA, E., LECOMTE, C. & BLESSING, R. H. (1995). *Acta Cryst.* B**51**, 661–668.
STEVENS, E. D., RYS, J. & COPPENS, P. (1977). *Acta Cryst.* A**33**, 333–338.
STEWART, R. F. (1969). *J. Chem. Phys.* **51**, 4569–4577.
STEWART, R. F. (1977). *Israel J. Chem.* **16**(2–3), 124–131.
STEWART, R. F. & FEIL, D. (1980). *Acta Cryst.* A**36**, 503–509.
STEWART, R. F., DAVIDSON, E. R. & SIMPSON, W. T. (1965). *J. Chem. Phys.* **42**, 3175–3187.
STRELTSOV, V. A., BELOKONEVA, E. L., TSIRELSON, V. G. & HANSEN, N. K. (1993). *Acta Cryst.* B**49**, 147–153.
SUNDERA-RAO, R. V. G., TURLEY, J. W. & PEPINSKY, R. (1957). *Acta Cryst.* **10**, 435–440.
SWAMINATHAN, S. & CRAVEN, B. M. (1984). *Acta Cryst.* B**40**, 511–518.
SWAMINATHAN, S., CRAVEN, B. M., SPACKMAN, M. A. & STEWART, R. F. (1984). *Acta Cryst.* B**40**, 398–404.
VEILLARD, A. (1968). *Theor. Chim. Acta*, **12**, 405.
WILLIS, B. T. M. & PRYOR, A. W. (1975). *Thermal Vibrations in Crystallography*. Cambridge Univ. Press.
WOLFRAM, W., ARUTUNIAN, E. G., ANTISHKINA, A. S. & PORAI-KOSHITS, M. A. (1967). *Bull. Acad. Pol. Sci. Sér. Sci. Chim.* **15**, 83–88.